Inorg. Chem. **2003**, *42*, 4568–4578

X- and Q-Band EPR Studies of the Dinuclear Mn(II) Complex $[(Bpmp)Mn_2(\mu\text{-}OAc)_2]^+$. Determination of the Spin Parameters for the $S = 1$ and $S = 2$ Spin States

Sébastien Blanchard,*,† Geneviève Blondin,*,† Eric Rivière,† Martine Nierlich,‡ and Jean-Jacques Girerd†

Laboratoire de Chimie Inorganique, UMR CNRS 8613, LRC-CEA n°33V, Institut de Chimie Moléculaire et des Matériaux d'Orsay, Université Paris-Sud, 91405 Orsay Cedex, France, and DRECAM/SCM Bat 125, CEA Saclay, 91191 Gif-sur-Yvette, France

Received March 19, 2003

A new μ-phenoxo-bis-μ-acetato di-Mn(II) complex using the BpmpH ligand was isolated as a perchlorate salt (BpmpH = 2,6-bis[bis(2-pyridylmethyl)aminomethyl]-4-methyl-phenol). The X-ray structure has been solved showing that the two Mn(II) ions are in a distorted octahedral environment. Investigation of the variation of the molar magnetic susceptibility upon temperature reveals an antiferromagnetic exchange interaction between the two high-spin Mn(II) ions. Fitting of the experimental data led to $g = 1.99$ and $J = 9.6$ cm^{-1} ($\hat{H}_{HDvV} = J\hat{S}_A \cdot \hat{S}_B$). EPR spectra recorded on a powder sample of $[(Bpmp)Mn_2(\mu\text{-}OAc)_2](ClO_4)\cdot 0.5H_2O$ at X-band between 4.3 K and room temperature and at Q-band between 5 and 298 K are presented. A new method based on a scrupulous examination of the variation upon temperature of these experimental spectra is developed here to first assign the transitions to the relevant spin states and second to determine the associated spin parameters. This approach is compared to the deconvolution process that has been previously applied to dinuclear Mn(II) complexes or metalloenzyme active sites. Crystallographic data is as follows: triclinic, space group $P\bar{1}$, $a = 10.154(2)$ Å, $b = 12.0454(2)$ Å, $c = 17.743(4)$ Å, $\alpha = 101.69(3)°$, $\beta = 93.62(3)°$, $\gamma = 94.67(3)°$, $Z = 2$.

Introduction

Manganese is involved in essential processes of life such as photosynthesis,[1] synthesis of DNA,[2] or the urea cycle.[3,4] Mononuclear in superoxide dismutases, the active sites of manganese-based metalloproteins expand up to tetranuclear in the water-oxidizing complex in the photosystem II of green plants. A great variety of oxidation states ranging from II to IV are easily accessible; Mn(V) is also invoked in several mechanism proposals.[5,6]

CW-EPR is a powerful spectroscopy that has been extensively used to investigate those active sites. Indeed, all the Mn oxidation states are paramagnetic. The first evidence for the presence of dimanganese(II,II) active site in arginase[7] or manganese catalases[8] emerged from EPR investigations: the X-ray diffraction studies later confirmed these conclusions.[9,10]

* Authors to whom correspondence should be addressed. E-mail: sblanchard@icmo.u-psud.fr (S.B.); gblondin@icmo.u-psud.fr (G.B.).
† Université Paris-Sud.
‡ CEA Saclay.

(1) Rutherford, A. W. *Philosophical Transactions issue on Photosystem II: molecular structure and function*; The Royal Society: London, 2002.
(2) Abbreviations used: DNA, deoxyribonucleic acid; CW, continuous wave; EPR, electron paramagnetic resonance; BpmpH, 2,6-bis(bis(2-pyridylmethyl)aminomethyl)-4-methyl-phenol; SVD, singular value decomposition; AcOH, acetic acid; L_1H, 2,6-bis(bis(2-pyridylethyl)-aminomethyl)-4-methyl-phenol; L_2H, 2,6-bis{(*N*-(2-dimethylamino-ethyl)-*N*-methyl)aminomethyl}-4-methylphenol; L_3H, 2,6-bis(*N*-(2-pyridylethyl)iminomethyl)-4-methylphenol; L_4H, 2,6-bis(2-(dimethyl-amino)ethyliminomethyl)-4-methylphenol; bompH, 2,6-bis(bis(2-meth-oxyethyl)aminomethyl)-4-methylphenol; L_5H, *N*,*N*,*N*′,*N*′-tetrakis(2-methylenebenzimidazolyl)-1,3-diaminopropan-2-ol; tmeda, *N*,*N*,*N*′,*N*′-tetramethylethylenediamine.
(3) Law, N. A.; Caudle, M. T.; Pecoraro, V. L. In *Advanced Inorganic Chemistry*; Sykes, G. B., Ed.; Academic Press: New York, 1998; Vol. 46, pp 305−440.
(4) *Manganese and Its Role in Biological Processes*; Marcel Dekker: New York, 2000; Vol. 37.
(5) Vrettos, J. S.; Limburg, J.; Brudvig, G. W. *Biochim. Biophys. Acta* **2001**, *1503*, 229−245.
(6) Dau, H.; Iuzzolino, L.; Dittmer, J. *Biochim. Biophys. Acta* **2001**, *1503*, 24−39.
(7) Reczkowski, R. S.; Ash, D. E. *J. Am. Chem. Soc.* **1992**, *114*, 10992−10994.
(8) Khangulov, S. V.; Barynin, V. V.; Voevodskaya, N. V.; Grebenko, A. I. *Biochim. Biophys. Acta* **1990**, *1020*, 305−310.
(9) Kanyo, Z. F.; Scolnick, L. R.; Ash, D. E.; Christianson, D. W. *Nature* **1996**, *383*, 554−557.

10.1021/ic0301066 CCC: $25.00
Published on Web 07/01/2003

Many efforts were developed in the past decade to deduce some structural information from detailed analyses of the EPR spectra of di-Mn(II) systems. In such systems, the two high-spin Mn(II) ions ($S_{Mn(II)} = {}^5/_2$) are in magnetic interaction, leading to a Heisenberg spin ladder where the total spin S ranges from 0 to 5. It has long been demonstrated that the observed EPR signatures result from the superposition of the paramagnetic $S = 1$ to $S = 5$ spin states.[11] Due to the weak antiferromagnetic exchange interaction that is common to most of the systems characterized so far, several excited spin states contribute to the EPR spectra, even below 40 K. Consequently, deconvolution processes based on singular value decomposition (SVD) were applied to extract the individual spin EPR spectrum originating from every involved paramagnetic states.[12,13] In addition to the individual S-spin state spectra, the coefficients that weighted the contribution of each spectrum to the one recorded are determined. In the deconvolution procedure, the main criterion that has to be fulfilled is the temperature dependence of those weighted coefficients that have to obey the Boltzmann law. In some works, this is the way the exchange coupling constant between the two Mn(II) ions is evaluated.[12,14] Only the $S = 2$ spectrum has been tentatively analyzed and the associated spin parameters evaluated.[12] It has been proposed that the zero-field splitting parameter $D_{S=2}$ correlates well with the Mn···Mn separation.

Recently, another approach based on the simulations of the EPR spectra recorded at X- and Q-bands was published.[15] To take into account the manganese hyperfine interactions (^{55}Mn, $I = {}^5/_2$, 100% natural abundance) detected on the frozen solution EPR spectra, analyses were focused on a selected number of the transitions contributing to the spectra.

We will report here a detailed investigation of the X- and Q-band powder spectra recorded on the dinuclear Mn(II) complex [(Bpmp)Mn$_2$(μ-OAc)$_2$](ClO$_4$) where BpmpH stands for 2,6-bis[bis(2-pyridylmethyl)aminomethyl]-4-methylphenol. This complex has been previously isolated as a powder with 0.5 additional water molecules per dinuclear unit[16] and we will report here for the first time the X-ray structure of the diethyl ether solvate. We will demonstrate that the powder spectra recorded between 6 and 30 K may be simulated with the two sole $S = 1$ and $S = 2$ temperature-independent signatures, the weighted factors allowing the determination of the exchange coupling constant. In addition, we will show that the sign of the zero-field splitting parameters may be deduced from the profile of the 4 K spectrum.

(10) Barynin, V. V.; Whittaker, M. M.; Antonyuk, S. V.; Lamzin, V. S.; Harrison, P. M.; Artymiuk, P. J.; Whittaker, J. W. *Structure* **2001**, *9*, 725−738.
(11) Laskowski, E. J.; Hendrickson, D. N. *Inorg. Chem.* **1978**, *17*, 457−470.
(12) Khangulov, S. V.; Pessiki, P. J.; Barynin, V. V.; Ash, D. E.; Dismukes, G. C. *Biochemistry* **1995**, *34*, 2015−2025.
(13) Meier, A. E.; Whittaker, M. M.; Whittaker, J. W. *Biochemistry* **1996**, *35*, 348−360.
(14) Antharavally, B. S.; Poyner, R. R.; Ludden, P. W. *J. Am. Chem. Soc.* **1998**, *120*, 8897−8898.
(15) Howard, T.; Telser, J.; DeRose, V. J. *Inorg. Chem.* **2000**, *39*, 3379−3385.
(16) Suzuki, M.; Mikuriya, M.; Murata, S.; Uehara, A.; Oshio, H.; Kida, S.; Saito, K. *Bull. Chem. Soc. Jpn.* **1987**, *60*, 4305−4312.

Table 1. Crystallographic Data for **1**(ClO$_4$)·(C$_2$H$_5$)$_2$O

empirical formula	$Mn_2C_{41}H_{49}ClN_6O_{10}$
fw	931.19
temp (K)	123(2)
wavelength (Å)	0.71073
cryst syst	triclinic
space group	$P\bar{1}$
a, Å	10.154(2)
b, Å	12.045(2)
c, Å	17.743(4)
α, deg	101.69(3)
β, deg	93.62(3)
γ, deg	94.67(3)
V, Å^3	2110.9(7)
Z	2
ρ_{calc}, g·cm^{-3}	1.465
μ, mm^{-1}	0.726
R1[a]	0.0632
wR2[b]	0.1433

[a] $R1 = \{\sum||F_o| - |F_c||\}/\{\sum|F_o|\}$. [b] $wR2 = \{\{\sum[w(F_o^2 - F_c^2)^2]^2\}/\{\sum[w(F_o^2)]^2\}\}^{1/2}$ with $w = 1/[\sigma^2(F_o^2) + (0.0744P)^2 + 1.1323P]$ where $P = (F_o^2 + 2F_c^2)/3$.

Experimental Section

General Remarks. Reagents and solvents were purchased commercially and used as received.

Caution: Perchlorates salts of metal complexes with organic ligands are potentially explosive. Only small quantities of these compounds should be prepared and handled behind suitable protective shields.

Synthesis. The BpmpH ligand was synthesized according to a previously reported procedure.[17] BpmpH (206 mg, 0.39 mmol, 1 equiv), Mn(OAc)$_2$·4H$_2$O (191 mg, 0.78 mmol, 2 equiv), and NaOAc (96 mg, 1.17 mmol, 3 equiv) were stirred for 30 min in open air in a methanol (8 mL)/water (1 mL) solution. An aqueous solution (0.5 mL) of NaClO$_4$ (95 mg, 0.78 mmol, 2 equiv) was then slowly added to the pale yellow mixture and a pale yellow precipitate formed immediately. Filtration yielded 140 mg (42%) of pure [(Bpmp)Mn$_2$(OAc)$_2$](ClO$_4$)·0.5H$_2$O. The infrared spectrum presented peaks at 1588.8, 1476.0, and 1428.3 cm^{-1} that can be attributed to vibrations of coordinated pyridines and acetates. The noncoordinated perchlorate anion is clearly identified by its 1086.4 and 763.5 cm^{-1} vibrations. Mass spectra acquired by ESI for [(Bpmp)Mn$_2$(OAc)$_2$](ClO$_4$)·0.5H$_2$O dissolved in acetonitrile show a peak at 757 mass units, consistent with the presence of the monocation [(Bpmp)Mn$_2$(OAc)$_2$]$^+$.

Elemental analysis. Calcd for $C_{37}H_{40}N_6O_{9.5}Mn_2Cl$: C, 51.31%; H, 4.66%; N, 9.70%. Found: C, 51.33%; H, 4.51%; N, 9.40%.

Infrared Spectroscopy. Spectra were recorded on KBr pellets in the range of 4000−200 cm^{-1} with a Perkin-Elmer Spectrum 1000 spectrophotometer.

Electrospray Ionization Mass Spectrometry. ESI mass spectra were acquired using a Quattro II (Micromass, Manchester, UK) triple quadrupole electrospray mass spectrometer operating in positive ion mode.

Elemental Analysis. Analyses were performed by the Service de Microanalyse of the CNRS (Gif sur Yvette, France) for carbon, nitrogen, and hydrogen.

Crystallographic Data Collection and Refinement of the Structure of 1(ClO$_4$)·(C$_2$H$_5$)$_2$O. The crystal data of **1**(ClO$_4$)·(C$_2$H$_5$)$_2$O and the parameters of data collection are summarized in Table 1. A colorless needle of approximate dimensions of 0.05 × 0.05 × 0.10 mm was selected. Diffraction collection was carried out on a Nonius diffractometer equipped with a CCD detector. The

(17) Lubben, M.; Feringa, B. L. *J. Org. Chem.* **1994**, *59*, 2227−2233.

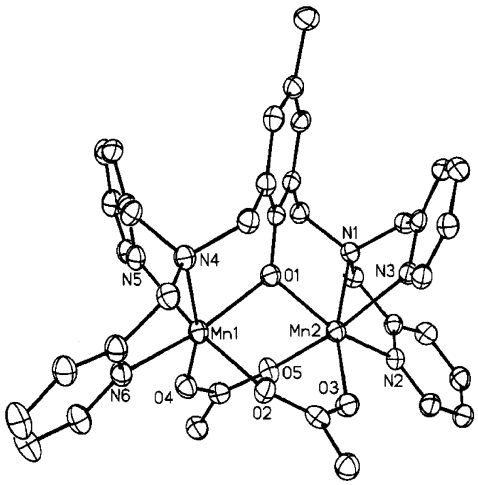

Figure 1. View of $[(Bpmp)Mn_2(\mu\text{-}OAc)_2]^+$ in **1**$(ClO_4)\cdot(C_2H_5)_2O$ showing the atom-labeling scheme.

lattice parameters were determined from 10 images recorded with 2° Φ-scans and later refined on all data. The data were recorded at 123 K. A 180° Φ-range was scanned with 2° steps with a crystal-to-detector distance fixed at 30 mm. Data were corrected for Lorentz polarization. The structure was solved by direct methods and refined by full-matrix least-squares on F^2 with anisotropic thermal parameters for all non-H atoms. All calculations were performed on an O2 Silicon Graphics Station with the SHELXTL package.[18] Crystal data are summarized in Table 1.

Magnetic Susceptibility Measurements. Magnetic susceptibility data were recorded on a MPMS5 magnetometer (Quantum Design Inc.). The calibration was made at 298 K using a palladium reference sample furnished by Quantum Design Inc. The data were collected over a temperature range of 2−300 K at a magnetic field of 0.1 T and were corrected for diamagnetism.

EPR Spectroscopy. X-band EPR spectra were recorded on Bruker 200D (X-band) and Bruker ELEXSYS 500 (X- and Q-band) spectrometers. For low-temperature studies, an Oxford Instrument continuous flow liquid helium cryostat and a temperature control system were used. At X-band the temperatures have been calibrated using a RhFe thermoresistance that was put inside a 5-mm quartz tube. All the simulations were performed using the XSophe software (4.0 version) developed by the department of Mathematics at the University of Queensland, Brisbane, Australia, and obtained from Brüker Analytik GmbH, Rheinstetten, Germany.

Results

Room-temperature diffusion of ether in a saturated acetonitrile solution of the isolated powder $[(Bpmp)Mn_2(\mu\text{-}OAc)_2](ClO_4)\cdot 0.5H_2O$ led to the formation of X-ray quality crystals as a solvated form $[(Bpmp)Mn_2(\mu\text{-}OAc)_2](ClO_4)\cdot(C_2H_5)_2O$.

X-ray Structure. Figure 1 shows a perspective view of the cation $[(Bpmp)Mn_2(\mu\text{-}OAc)_2]^+$. Selected distances and angle are listed in Table 2. The two manganese ions are bridged by the phenoxy oxygen of the $Bpmp^-$ ligand and by two acetate groups in a *syn*−*syn* conformation, affording a μ-phenoxo-bis(μ-carboxylato)dimanganese(II) core structure. The phenoxy oxygen is symmetrically bonded to the two manganese sites whereas the two acetate groups are unsymmetrically bridging as evidenced by the $Mn-O_{acetato}$ bond lengths: the Mn1−O2 and Mn2−O5 distances of 2.158(4) and 2.148(4) Å, respectively, are longer than the Mn1−O4 and Mn2−O3 separations of 2.095(4) and 2.114(4) Å, respectively. This was also observed in the closely related $[(L_1)Mn_2(\mu\text{-}OAc)]^+$ complex (**2**).[19] The two Mn(II) ions are in a distorted octahedral environment with a *cis*−*cis* O_3N_3 coordination. The Mn−O and Mn−N bond lengths are in the range usually observed for Mn(II) complexes. The $Mn-N_{amine}$ bond lengths (Mn1−N4 2.331(4), Mn2−N1 2.320(4) Å) are slightly longer than the $Mn-N_{pyridine}$ distances (Mn1−N5 2.295(4), Mn1−N6 2.267(4), Mn2−N3 2.311(4), Mn2−N2 2.298(4) Å) and the shortest $Mn-N_{pyridine}$ (N6 or N2) bond length on one site involves the pyridine group trans to the bridging phenoxy oxygen. These structural features seem to be characteristic of the ligation of the $Bpmp^-$ ligand to a Mn(II) ion since they are also observed in the mixed valent complexes $[(Bpmp)Mn_2(\mu\text{-}O_2CCH_3)_2]^{2+}$ (**3**)[20] and $[(Bpmp)Mn_2(\mu\text{-}O_2CC_6H_5)_2]^{2+}$ (**4**).[16] The μ-phenoxo-bis(μ-acetato)-dimanganese(II) core structure in **1** presents a more bent Mn1−O1−Mn2 bridging angle (107.9(1)°) compared to the corresponding mixed valent Mn(II)Mn(III) systems **3** and **4** or to di-Mn(II) complexes **2** and $[(CH_3OH)Mn(L_2)(\mu\text{-}O_2CC_6H_5)_2Mn(NCS)]^+$ (**5**)[21] (114.4(2), 116.6(5), 115.8, and 113.5°, respectively). The bridging angle value is however greater than those determined in μ-phenoxo-bis(μ-acetato)-dimanganese(II) complexes where one metallic site is pentacoordinated: 99.9(2) and 100.6(2)° in $[(L_3)Mn_2(\mu\text{-}OAc)_2(NCS)]$ (**6**),[22] 101.9° in $[(L_3)Mn_2(\mu\text{-}OAc)_2(CH_3OH)](ClO_4)$ (**7**),[23] and 101.2° in $[(L_4)Mn_2(\mu\text{-}OAc)_2(NCS)]$ (**8**).[24] However, a similar value (107.3°) is observed in $[Mn_2(bomp)(PhCO_2)_2](BPh_4)$ (**9**).[25] The 3.412(1)-Å Mn···Mn separation determined here, close to the one in **9** (3.3892(7) Å), thus lies between the short Mn···Mn distance in **6**, **7**, and **8** (3.337(2), 3.344(2) Å in **6**, 3.366(2) Å in **7** and 3.325(3) Å in **8**) and the long metal−metal separation in **2** and **5** (3.589(3) and 3.598(4) Å, respectively).

Table 2. Selected Distances (Å) and Angle (deg) for $[(Bpmp)Mn_2(\mu\text{-}OAc)_2](ClO_4)\cdot(C_2H_5)_2O$

Mn1−O1	2.103(3)	Mn2−O1	2.117(3)
Mn1−O2	2.158(4)	Mn2−O3	2.114(4)
Mn1−O4	2.095(4)	Mn2−O5	2.148(4)
Mn1−N6	2.267(4)	Mn2−N2	2.298(4)
Mn1−N5	2.295(4)	Mn2−N1	2.320(4)
Mn1−N4	2.331(4)	Mn2−N3	2.311(4)
Mn1···Mn2	3.412(1)	Mn1−O1−Mn2	107.9(1)

Magnetic Susceptibility Measurements. As a complementary investigation to the EPR study of complex **1**, we have reinvestigated the variation of the molar magnetic

(18) Sheldrick, G. M. *SHELXTL*−*Program for the Refinement of Crystal Structure*; University of Göttingen: Göttingen, Germany, 1997.

(19) Gultneh, Y.; Farooq, A.; Liu, S.; Karlin, K. D.; Zubieta, J. *Inorg. Chem.* **1992**, *31*, 3607−3611.

(20) Diril, H.; Chang, H.-R.; Zhang, X.; Larsen, S. K.; Potenza, J. A.; Pierpont, C. G.; Schugar, H. J.; Isied, S. S.; Hendrickson, D. N. *J. Am. Chem. Soc.* **1987**, *109*, 6207−6208.

(21) Higuchi, C.; Sakiyama, H.; Okawa, H.; Fenton, D. E. *J. Chem. Soc., Dalton Trans.* **1995**, 4015−4020.

(22) Mikuriya, M.; Fujii, T.; Kamisawa, S.; Kawasaki, Y.; Tokii, T.; Oshio, H. *Chem. Lett.* **1990**, 1181−1184.

(23) Mikuriya, M.; Fujii, T.; Tokii, T.; Kawamori, A. *Bull. Chem. Soc. Jpn.* **1993**, *66*, 1675−1686.

(24) Sakiyama, H.; Tamaki, H.; Kodera, M.; Matsumoto, N.; Okawa, H. *J. Chem. Soc., Dalton Trans.* **1993**, 591−595.

(25) Sakiyama, H.; Sugawara, A.; Sakamoto, M.; Unoura, K.; Inoue, K.; Yamasaki, M. *Inorg. Chim. Acta* **2000**, *310*, 163−168.

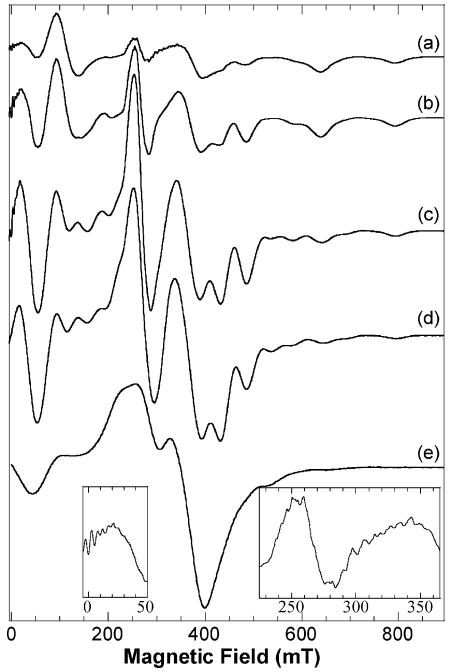

Figure 2. Selected X-band spectra recorded on a powder sample of **1**$(ClO_4)\cdot 0.5H_2O$: (a) 4.3 K, (b) 9.2 K, (c) 18.0 K, (d) 28.2 K, and (e) 100 K. EPR conditions for spectra a−d: 9.4263 GHz microwave frequency, 0.507 mW microwave power, 0.5 mT modulation amplitude, 100 kHz modulation frequency. EPR conditions for spectrum (e): 9.3886 GHz microwave frequency, 0.797 mW microwave power, 0.5 mT modulation amplitude, 100 kHz modulation frequency. Only the intensities of spectra a−d may be compared. Insert: Expansions of the 4.3 K spectrum between −5 and 50 mT (left) and 225 and 375 mT (right), respectively.

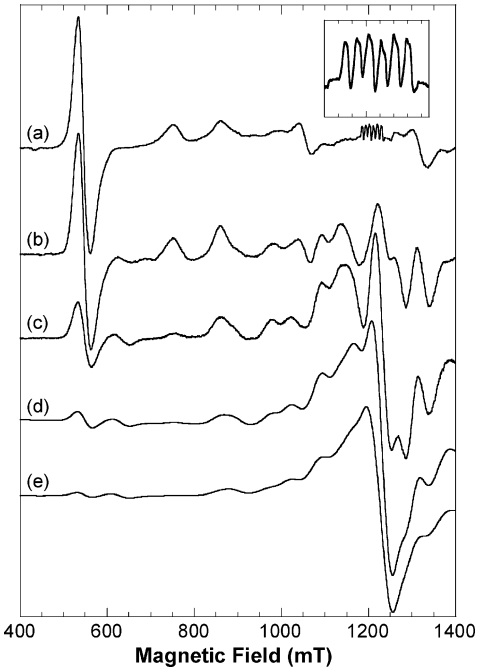

Figure 3. Selected Q-band spectra recorded on a powder sample of **1**$(ClO_4)\cdot 0.5H_2O$: (a) 5 K, (b) 10 K, (c) 25 K, (d) 50 K, and (e) 80 K. EPR conditions for spectra a−e: 34.0 GHz microwave frequency, 55.4 μW (spectra a and b) or 2.23 mW (spectra c−e) microwave power, 0.5 mT modulation amplitude, 100 kHz modulation frequency, 1 (spectra c−e) or 4 (spectra a and b) scans. Spectra c−e were scaled to the recording conditions of spectra a and b. In addition, spectra d and e are divided by 8 and 16 respectively for presentation purposes.

susceptibility χ_M upon temperature. The $\chi_M T$ product measured on a powder sample of **1**$(ClO_4)\cdot 0.5H_2O$ decreases from 7.47 $cm^3\cdot mol^{-1}\cdot K$ at 295 K down to 0.008 $cm^3\cdot mol^{-1}\cdot K$ at 2 K (see Figure S1). This behavior indicates a weak antiferromagnetic exchange interaction between the two high-spin Mn(II) ions ($S_A = S_B = {}^5/_2$), leading to a diamagnetic $S = 0$ ground state. Using the Heisenberg−Dirac−van Vleck Hamiltonian given in eq 1 and the van Vleck formula, the best fit was obtained with $J = 9.6$ cm^{-1} and $g = 1.99$ (see Figure S1).

$$\hat{H}_{HDvV} = J\hat{S}_A\cdot\hat{S}_B \qquad (1)$$

These values are similar to the ones previously published ($J = 9.8$ cm^{-1} and $g = 2.00$)[16] and are in good agreement with those reported in the literature for similar dinuclear Mn(II) complexes presenting the μ-phenolato-di-μ-carboxylato core structure (from 5 to 11 cm^{-1}).[21−26]

Powder EPR Spectra. (a) Description. The X- and Q-band EPR spectra of powder samples of **1**$(ClO_4)\cdot 0.5H_2O$ were recorded between 4.3 K and room temperature under nonsaturated conditions. A selection is presented in Figures 2 and 3. The 9.4 GHz and 4.3 K spectrum exhibits features between 0 and 800 mT. Transitions at 20 and 265 mT present additional lines separated by 4.5 mT (see inserts in Figure 2). Six lines separated by 9 mT are also detected at 335 mT. These six lines originate from a highly diluted Mn(II) monomeric impurity that we will ignore in the forthcoming analysis. Upon increasing of the temperature, the resonances detected at 4.3 K vary in their relative intensities and additional features are detected. Intensity is lost in the high field wing of the spectrum while an important gain in the $g = 2$ region (∼335 mT) is seen. At room temperature, only a broad feature centered at 335 mT is detected (not shown). The EPR spectrum recorded at 34.0 GHz and 5 K present five well-defined transitions between 0.5 and 1.4 T. As in X-band, six well-resolved lines separated by 8.9 mT and centered at $g = 2$ (1.207 T) are indicative of the presence of a diluted Mn(II) monomeric impurity. The increase of the temperature induces changes similar to those observed at X-band, that is, the appearance of new transitions that produce a gain in intensity in the $g = 2$ region. The room-temperature Q-band spectrum (not shown) is very similar to the one published by Mathur et al. recorded at 140 K on the complex $[L_5Mn_2(OH)Br_2]$.[27]

(b) Theoretical Tools. As previously mentioned in the literature, this strong temperature dependence of the EPR spectra is due to the weak exchange coupling between the two Mn(II) paramagnetic centers A and B with local electronic spins $S_A = S_B = {}^5/_2$. The following Hamiltonian may be written,[28]

$$\hat{H} = \hat{H}_A + \hat{H}_B + \hat{H}_{AB} \qquad (2)$$

(26) Higuchi, C.; Sakiyama, H.; Okawa, H.; Isobe, R.; Fenton, D. E. *J. Chem. Soc., Dalton Trans.* **1994**, 1097−1103.

(27) Mathur, P.; Crowder, M.; Dismukes, G. C. *J. Am. Chem. Soc.* **1987**, *109*, 5227−5233.

where for i = A or B

$$\hat{H}_i = \mu_B \hat{B}_0 \tilde{g}_i \hat{S}_i + \hat{S}_i \tilde{D}_i \hat{S}_i + \hat{I}_i \tilde{a}_i \hat{S}_i \quad (3)$$

and

$$\hat{H}_{AB} = \hat{S}_A \tilde{J}_{AB} \hat{S}_B \quad (4)$$

The first, second, and third terms in eq 3 are the Zeeman effect, the zero-field splitting, and the hyperfine interaction ($I_{Mn} = {}^5/_2$) on each paramagnetic center, respectively. The isotropic component of the Hamiltonian $\hat{H}_{AB}$ corresponds to the Heisenberg−Dirac−van Vleck exchange interaction while the anisotropic part reproduces the antisymmetric exchange interaction and the dipolar coupling.

When the isotropic exchange interaction is the leading term in eq 2, the total electronic spin S ($|S_A - S_B| \leq S \leq S_A + S_B$) is a good quantum number. The EPR signature of each S-spin state relies on the Hamiltonian $\hat{H}_S$:[28]

$$\hat{H}_S = \mu_B \hat{B}_0 \tilde{g}_S \hat{S} + \hat{S} \tilde{D}_S \hat{S} + \sum_{i=A,B} \hat{I}_i \tilde{A}_S^{\,i} \hat{S} \quad (5)$$

The first, second, and third terms in eq 5 stand for the Zeeman effect, the zero-field splitting, and the hyperfine interactions for the S-spin state, respectively. The tensors in eq 5 are related to the local tensors written in eqs 3 and 4 (vide infra).[28]

The Zeeman effect at X- or Q-band is at least 1 order of magnitude smaller than the isotropic exchange interaction. This allows the use of eqs 1 and 5 to analyze the EPR spectra presented here. Within this framework, any experimental spectrum recorded at the temperature T may be reproduced by a linear combination of the individual S-spin state spectra with temperature-dependent weighted coefficients. If the thermal energy is larger than the eigenvalues of $\hat{H}_S$, the intensity of any individual S-spin state spectrum follows a Curie law so one can write the following relation,

$$Y(\nu,B,T) = \sum_S \frac{n_S(T)}{T} Y_S(\nu,B) \quad (6)$$

where $Y(\nu,B,T)$ is the experimental spectrum recorded at ν frequency, $Y_S(\nu,B)$ is the temperature-independent spectrum of the S-spin state calculated at frequency ν, and $n_S(T)$, given by eq 7, is the Boltzmann population of any Zeeman level of the considered S-spin state evaluated at zero field:

$$n_S(T) = \frac{\exp\left[-\dfrac{JS(S+1)}{2k_BT}\right]}{\displaystyle\sum_{S'=0}^{5} (2S'+1) \exp\left[-\frac{JS'(S'+1)}{2k_BT}\right]} \quad (7)$$

Equation 6 indicates that the contribution of the individual S-spin state spectrum $Y_S(\nu,B)$ to the experimental one $Y(\nu,B,T)$ is $n_S(T)/T$. Due to the J value, one may expect that the spectra recorded at temperatures lower than 10 K originate only from the $S = 1$ and $S = 2$ spin states, the other excited spin states not being populated (see Figure S2).

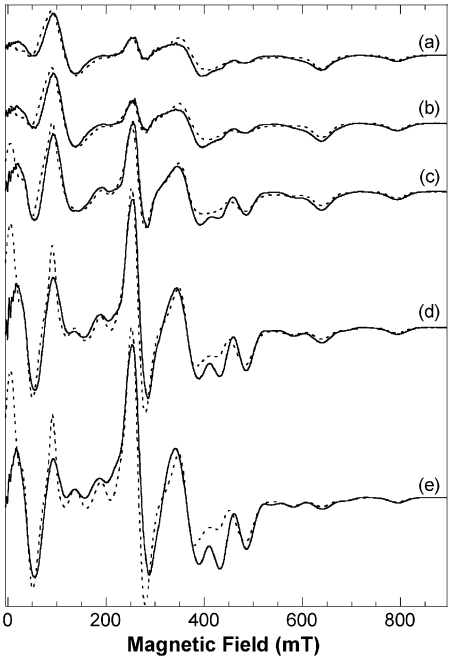

Figure 4. Experimental (continuous line) and simulated (dotted line) X-band spectra at several temperatures: (a) 4.3 K, (b) 6.8 K, (c) 9.2 K, (d) 13.8 K, (e) 18.0 K. All spectra were scaled to the recording conditions of spectrum (a). See text for the simulated spectra.

(c) Transition Assignment. Whatever the spin state is, the electronic density is equally spread on the two manganese ions. Within the S-spin state, if the zero-field splitting effect is small compared to the isotropic exchange interaction, one can establish the following relation (i = A,B):[28]

$$\hat{A}_S^{\,i} = \frac{1}{2}\tilde{a}_i \quad (8)$$

The hyperfine interaction with the two equivalent $I = {}^5/_2$ manganese nuclei thus leads to the subdivision of one EPR transition into 11 lines in a 1:2:3:4:5:6:5:4:3:2:1 pattern. The lines are equally separated by 4.5 mT, that is, half the value usually observed in mononuclear Mn(II) system. The structure detected at 4.3 K and X-band on the 20 and 265 mT transitions is thus the signature of the hyperfine interaction between the electronic spin S with two equivalent Mn nuclei (see inserts in Figure 2). Because the sample investigated here is a powder, it is remarkable to detect a so well-resolved hyperfine structure. Indeed, the paramagnetic species has to be diluted to observe the hyperfine interactions; otherwise, the EPR lines are broadened due to dipolar interactions between the paramagnetic centers. This suggests that the involved electronic spin level is very weakly populated. The fact that this hyperfine structure disappears upon increasing temperature suggests that those lines originate from the $S = 2$ spin state. This assignment is confirmed by the important gain in intensity of those lines when increasing the temperature from 4.3 to 13.8 K (see Figure 4). A detailed examination of those two X-band spectra reveals that a similar behavior is observed for the lines centered at 180, 430, 482, 580, and

(28) Bencini, A.; Gatteschi, D. *EPR of Exchange Coupled Systems*; Springer-Verlag: Berlin, 1990.

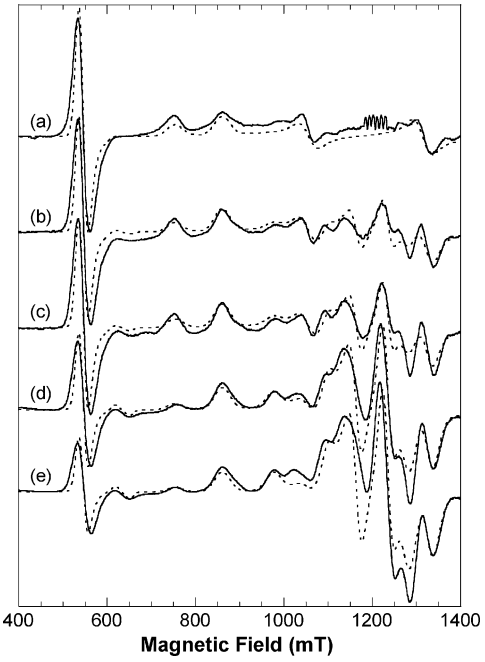

Figure 5. Experimental (continuous line) and simulated (dotted line) Q-band spectra at several temperatures: (a) 5 K, (b) 8 K, (c) 10 K, (d) 15 K, and (e) 20 K. All spectra were scaled to the recording conditions of spectrum (a). See text for the simulated spectra.

780 mT. They thus all originate from the $S = 2$ spin state. The identification of the $S = 2$ transitions leads to the determination of the EPR spectrum originating from the triplet state. It consists at X-band in four transitions located at 112, 373, 639, and 794 mT. Such a pattern is obtained when the zero-field splitting effect is slightly larger than the energy quantum associated with the recording frequency ($\nu_X = 9.43$ GHz, $\nu_X/100c = 0.3$ cm^{-1}). No hyperfine structure was detected at Q-band that would help in the assignment of the transitions. Nevertheless, the 5 K spectrum is fully consistent with that one can expect for a triplet state presenting a zero-field splitting effect smaller than the energy quantum ($\nu_Q = 34.0$ GHz, $\nu_Q/100c = 1.2$ cm^{-1}).

(d) Simulations. Simulations of the EPR spectra recorded at both X- and Q-bands at temperatures lower than 30 K are shown in Figures 4 and 5 (see also Figure S3). Due to the high value of the manganese nuclear spin, the hyperfine interactions were ignored. The Hamiltonian written in eq 5 thus reduces to

$$\hat{H}_S = g_S \mu_B \hat{B}_0 \cdot \hat{S} + D_S\left[\hat{S}_z^2 - \frac{1}{3}S(S+1)\right] + E_S[\hat{S}_x^2 - \hat{S}_y^2] \quad (9)$$

where the zero-field splitting contribution has been developed according to the usual formulation.

One of the key points of the proposed simulations rests on the use at both X- and Q-bands of a single set of spin parameters. The values are listed in Table 3. The $\tilde{g}_{S=1}$ and $\tilde{g}_{S=2}$ tensors were assumed to be isotropic with principal values equal to 2. The use of temperature-independent traces $Y_S(\nu,B)$ does not allow the determination of the sign of the D_S parameters. However, the negative sign of $D_{S=1}$ and $D_{S=2}$ (see Table 3) will be justified in the next section. The given uncertainties correspond to a significant (5 mT at least)

Table 3. Spin Parameters of the $S = 1$ and $S = 2$ Spectra Calculated at 9.4263 and 34.0 GHz

	D_S (in cm^{-1})	E_S/D_S	g_{iso}	$\omega_x, \omega_y, \omega_z$ (in Gauss)[a]
$S = 1$	-0.428 ± 0.004	0.150 ± 0.005	2	200, 200, 200
$S = 2$	-0.110 ± 0.005	0.125 ± 0.005	2	125, 200, 200

[a] Half-width at half-height assuming a Gaussian line shape.

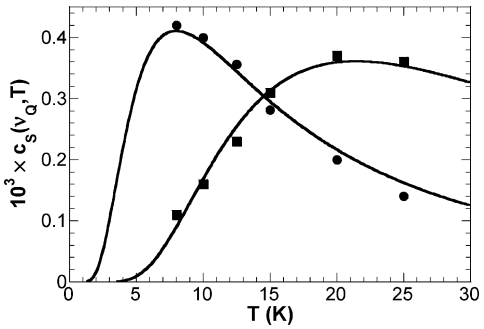

Figure 6. Variation upon temperature of the contribution coefficients plotted as $10^3\ c_S(\nu_Q,T)$ determined at Q-band for the $S = 1$ (full circles) and $S = 2$ (full squares) with the theoretical curves $\alpha_{S=1}(\nu_Q) \times n_{S=1}(T)/T$ and $\alpha_{S=2}(\nu_Q) \times n_{S=2}(T)/T$ (solid lines) calculated with $J = 9.4$ cm^{-1}, $\alpha_{S=1}(\nu_Q) = 0.028$ and $\alpha_{S=2}(\nu_Q) = 0.181$.

displacement of the calculated lines in comparison with the experimental ones. X- and Q-band spectra are better reproduced when considering an anisotropic line width within the $S = 2$ state. It may be related to the hyperfine interactions that have been discarded.[29] The X-band 4.3 K spectrum indeed shows that the hyperfine structure is not resolved in all the $S = 2$ transitions.

The XSophe program allows the calculation of temperature-independent individual spin state spectra. However, the most intense peak is arbitrarily set to 10^8. This led us to introduce a scaling factor $\alpha_S(\nu)$ (T and B independent) defined according to

$$Y_S(\nu,B) = \alpha_S(\nu) Y_S^{\text{XSophe}}(\nu,B) \quad (10)$$

The proposed simulations are obtained using linear combinations of the XSophe computed $S = 1$ and the $S = 2$ spectra. The individual spectra are shown in Figure 7 and the $c_{S=1}(\nu,T)$ and $c_{S=2}(\nu,T)$ coefficients defined according to eq 11 will be discussed below.

$$Y(\nu,B,T) = c_{S=1}(\nu,T) Y_{S=1}^{\text{XSophe}}(\nu,B) + c_{S=2}(\nu,T) Y_{S=2}^{\text{XSophe}}(\nu,B) \quad (11)$$

According to eqs 6, 7, and 10, the $c_{S=1}(\nu,T)$ (respectively $c_{S=2}(\nu,T)$) coefficient depends on the exchange coupling constant J and on the scaling factor $\alpha_{S=1}(\nu)$ (respectively $\alpha_{S=2}(\nu)$). To reproduce a series of spectra recorded at a single microwave frequency, two different procedures may be adopted depending on the assumption that the J-value is known or not. In a first approach followed at X-band, we assumed a J-value of 9.6 cm^{-1} as deduced from the magnetic susceptibility measurements. Consequently, only the scaling factors were unknown and could indeed be determined from a single simulated spectrum. The 9.2 K

(29) Mabbs, F. E.; Collison, D. *Electron Paramagnetic Resonance of d Transition Metal Compounds*; Elsevier Science Publishers B. V.: Amsterdam, The Netherlands, 1992; Vol. 16.

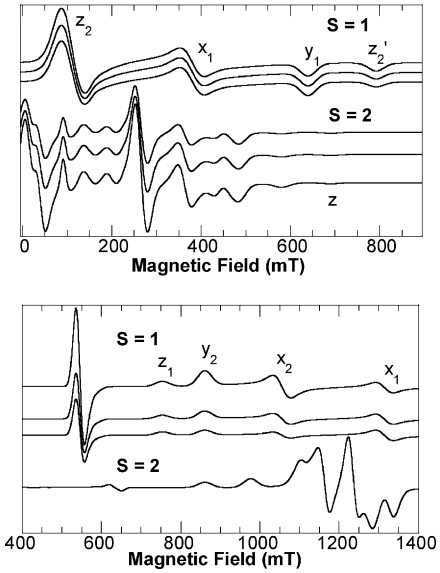

Figure 7. X-band (top) and Q-band (bottom) spectra calculated for $S = 1$ (three upper traces) and $S = 2$ (three or single bottom traces) considered as isolated spin states with the spin parameters listed in Table 3. Middle or single traces: Temperature-independent spectra scaled in such a way that the summation gives the simulated X-band-9.2 K (trace c in Figure 4) and Q-band-15 K (trace d in Figure 5) spectra, respectively. Lower ($D_S < 0$) and upper ($D_S > 0$) traces: 9.4 GHz, 4.3 K, $S = 1$; 9.4 GHz, 4.3 K, $S = 2$; and 34 GHz, 4 K, $S = 1$ calculated spectra scaling to the temperature-independent traces according to the $S = 1$ x_1-line or to the $S = 2$ z-line. The x, y, and z labeling transitions refer to a positive E_S/D_S ratio. The subscript 1 (respectively 2) refers to a transition between the two lowest (respectively highest) levels within the triplet state for a negative $D_{S=1}$ parameter.

spectrum at X-band was chosen to determine the best linear combination (according to eye looking) of the $S = 1$ and $S = 2$ temperature-independent spectra, $Y_{S=1}^{\text{XSophe}}(\nu_X,B)$ and $Y_{S=2}^{\text{XSophe}}(\nu_X,B)$ (trace c in Figure 4), leading to the following scaling factor values: $\alpha_{S=1}(\nu_X) = 0.107$ and $\alpha_{S=2}(\nu_X) = 2.653$. Simulations of the spectra recorded at $T = 6.8$, 13.8, 18.0, and 28.2 K were then obtained as linear combinations of $Y_{S=1}(\nu_X,B)$ and $Y_{S=2}(\nu_X,B)$ with the calculated weighted coefficients $n_{S=1}(T)/T$ and $n_{S=2}(T)/T$. The obtained traces indeed reproduce almost perfectly the recorded spectra, validating the theoretical equations used to express the temperature dependence of the EPR spectra of the dinuclear Mn(II) complex along with the spin parameter values used to calculate the 9.4 GHz individual $S = 1$ and $S = 2$ spectra.

This first result allows one to go one step further and to determine the exchange coupling constant from the temperature dependence of the coefficients used in the linear combinations of the computed $S = 1$ and $S = 2$ spectra. This procedure was followed at Q-band. In a first step, the 8−25 K spectra were simulated (eye looking) using linear combinations of the temperature-independent $Y_{S=1}^{\text{XSophe}}(\nu_Q,B)$ and $Y_{S=2}^{\text{XSophe}}(\nu_Q,B)$ spectra. The obtained $c_{S=1}(\nu_Q,T)$ and $c_{S=2}(\nu_Q,T)$ coefficients are reported in Figure 6 as functions of T. In a second step, the fitting procedure performed simultaneously on the two contribution factors led to the following values: $J = 9.4$ cm^{-1}, $\alpha_{S=1}(\nu_Q) = 0.028$ and $\alpha_{S=2}(\nu_Q) = 0.181$ (see Figure 6). The obtained J-value is indeed fully in agreement with the value determined from the magnetic susceptibility measurements.

(e) D_S-Sign Determination. In the previous series of simulated spectra, the 4.3 K X-band and the 5 K Q-band traces (see Figures 4 and 5) have been obtained using a procedure slightly different from the one above that will be explained now. Indeed, a detailed examination of these two experimental spectra reveals temperature effects *within the spin states*.

The intensity of one EPR transition within one individual S-spin state is proportional to the population difference between the two levels (designated "a" and "b", respectively) involved in the transition,

$$I_{ab} = I_0 \frac{\exp\left[-\frac{E_a}{k_B T}\right] - \exp\left[-\frac{E_b}{k_B T}\right]}{\sum_j \exp\left[-\frac{E_j}{k_B T}\right]} \qquad (12)$$

where the summation runs over all the energy levels, E_j standing for the eigenvalues of the Hamiltonians $\hat{H}_S$ ($S = 0-5$) expressed in eq 5 corrected from the exchange contribution. Because of the EPR transition occurring between the "a" and "b" levels, one has $E_b - E_a = h\nu$. If the thermal energy is smaller than the eigenvalues E_j, the population difference depends on the couple of levels considered within one S-spin state. Consequently, some transitions are decreased or even not visible. Such a situation is frequently observed in high-field high-frequency EPR experiments.

In the present instance, the 5 K Q-band spectrum exhibits a less intense 1.055 T line in comparison with the 1.315 T one. In the temperature-independent spectrum, both transitions are of the same intensity. This intensity difference is thus the signature of temperature effects *within the spin states*, which allows for the determination of the sign of $D_{S=1}$. Indeed, those lines correspond to the transitions expected when the magnetic field is aligned along the x-direction of the zero-field splitting tensor $\tilde{D}_{S=1}$. Figure 7 shows the variation in intensity expected at 4 K for a positive or a negative $D_{S=1}$ parameter compared to the temperature-independent trace. The three spectra are scaled to the x_1-line to better visualize the relative intensities of the x_1- and x_2-lines. Figure S4 depicts the variations of the energy levels of a triplet state as a function of the applied magnetic field when aligned along the principal directions of the zero-field splitting tensor. For a negative $D_{S=1}$ parameter, the x_1-line (respectively x_2-line) corresponds to a transition between the two lowest (respectively highest) Zeeman levels of the triplet state. Consequently, the greatest population difference is associated with the x_1-line, which indeed exhibits a greater intensity compared to the x_2-line. For a positive $D_{S=1}$ parameter, the x_1-line now involves the two highest Zeeman levels of the S=1 spin state. Therefore, the x_1-line is less intense than the x_2-line. The experimental relative line intensities thus suggest a negative $D_{S=1}$ parameter.[30] This sign is confirmed by the X-band profile observed at 4.3 K. If the simulated spectrum based on the temperature-independent $Y_{S=1}(\nu_X,B)$ contribution is scaled to fit the 640

mT line experimentally observed, the line at 371 mT is then correctly reproduced in intensity while the lines at 115 and 792 mT of the simulated spectrum are too intense compared to the experimental data. These last two transitions are indeed associated with the *z*-transitions within the triplet state, the *z*-axis being the distortion axis of the zero-field splitting tensor $\tilde{D}_{S=1}$ while the two former correspond to the *y*- and *x*-transitions, respectively (see Figure 7). For a negative $D_{S=1}$ parameter, these *z*-transitions involve the two highest Zeeman levels within the triplet state while a positive $D_{S=1}$ value implies the two lowest. The reverse situation occurs for the *x*- and *y*-lines: the transition occurs between the two lowest Zeeman levels if $D_{S=1}$ is negative and the two highest if $D_{S=1}$ is positive. These differences are at the origin of the changes in relative line intensities shown in Figure 7. The negative sign of the $D_{S=1}$ parameter is thus also clearly established at X-band, comparing the relative intensities of the *x*- and *y*-transitions on one hand and those of the *z*-transitions on the other. The Q-band 5 K spectrum is satisfyingly reproduced with the 4 K computed triplet signature without any contribution of the $S = 2$ spin state while for the X-band 4.3 K spectrum, a combination of the $S = 1$ and $S = 2$ spectra both computed at 4.3 K is used.

As a temperature effect is clearly detected for the $S = 1$ spin state signature, a similar effect should be present on the $S = 2$ signal. But due to the smaller magnitude of the $D_{S=2}$ parameter, it may be more difficult to observe at X- or Q-band. In addition, the superimposition of some of the $S = 2$ lines with those of the $S = 1$ signal is a strong disadvantage. At 34.0 GHz, the 5 K spectrum has no contribution from the $S = 2$ spin state and the 8 K spectrum was well-reproduced with the temperature-independent computed traces. In this respect, Q-band is of no help. On the other hand, if one considers the calculated 4.3 K $S = 1$ signal and the temperature-independent $Y_{S=2}(\nu_X,B)$ trace weighted by the appropriate $n_{S=2}(T)/T$ value to reproduce the 4.3 K X-band spectrum, the lines at 20 and 250 mT that originate from the $S = 2$ spin state are underestimated by at least a factor of 10. This strongly suggests that a temperature effect is present within the $S = 2$ signature. Figure 7 shows the effect on the 4.3 K X-band $S = 2$ signal of a positive or a negative $D_{S=2}$ parameter compared to the temperature-independent profile. The three spectra are scaled in such a way that the 690 mT *z*-lines superimpose. In comparison with the temperature-independent trace, a negative sign clearly leads to an enhancement of the entire spectrum while a positive value reduces it. This entails us to favor a negative value for $D_{S=2}$. The simulated 4.3 K 9.4 GHz spectrum is thus based on the 4.3 K $S = 1$ signal along with the $S = 2$ signature calculated at the same temperature with both D_S spin parameters of negative sign.

(f) $S = 3$ Contribution. The proposed simulated spectra at 13.8, 18.0, and 28.2 K at X-band and 15, 20, and 25 K at Q-band (see Figures 4, 5, and S3) clearly do not reproduce all the detected transitions. As already mentioned, the $S = 3$ state can no longer be neglected at temperatures higher than 10 K. At X-band, the lines at 220 (shoulder), 432, and 538 mT can clearly be attributed to the $S = 3$ state. At Q-band, the $S = 3$ signature appears at least at 1.03 T and as a shoulder at 1.17 T. This suggests that the zero-field splitting effect in the $S = 3$ state is weaker than those in the $S = 1$ and $S = 2$ states but the precise determination of the spin parameters is very subtle and we postpone it to a further investigation.

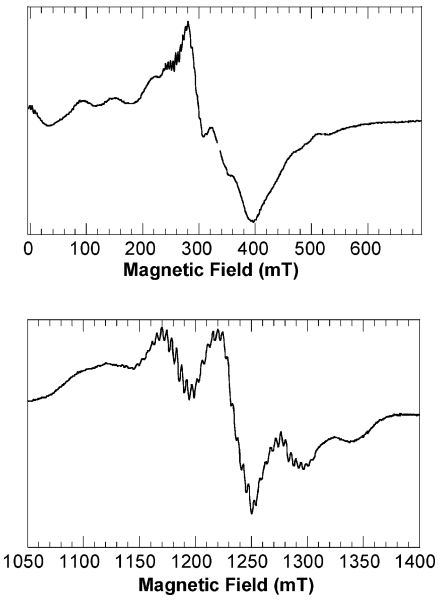

Figure 8. X- (top) and Q- (bottom) band spectra recorded on a frozen acetonitrile solution of **1**$(ClO_4)\cdot(C_2H_5)_2O$. X-band EPR conditions: 9.3845 GHz microwave frequency, 2.007 mW microwave power, 0.5 mT modulation amplitude, 100 kHz modulation frequency, $T = 100$ K. Q-band EPR conditions: 34.0 GHz microwave frequency, 2.095 mW microwave power, 0.5 mT modulation amplitude, 100 kHz modulation frequency, $T = 25$ K.

Frozen Solution EPR Spectra. The EPR spectra were also recorded on frozen solutions using a solution of tetrabutylammonium perchlorate, 0.1 M, in acetonitrile as solvent. Representative spectra are shown in Figure 8. At X-band and 100 K, a hyperfine structure is detected from 0 up to 430 mT with better resolution between 0 and 20 mT (6 lines) and between 220 and 320 mT (18 lines). Only 11 lines were detected on the recently reported 10 K X-band spectrum.[31] The separation between the lines varies from 3.7 to 4.5 mT, indicating the maintenance in solution of the dinuclear Mn(II) structure. A similar pattern has been previously observed on model complexes[15,19,32−34] as on metalloproteins such as catalases,[12,13] arginase,[7] concanavalin A,[35] and enolase.[36] Q-band EPR spectra were recorded between 5 and 80 K. At 5 K, only the signature of the $S = 1$ state was seen in agreement with solid state measurements. No hyperfine structure was detected especially in the 545

(30) The E_S parameter is chosen such that it has the same sign as the D_S parameter, allowing a univocal labeling of the transition whatever the sign of D_S.

(31) Huang, P.; Magnuson, A.; Lomoth, R.; Abrahamsson, M.; Tamm, M.; Sun, L.; van Rotterdam, B.; Park, J.; Hammarström, L.; Åkermark, B.; Styring, S. *J. Inorg. Biochem.* **2002**, *91*, 159−172.
(32) Mabad, B.; Cassoux, P.; Tuchagues, J.-P.; Hendrickson, D. N. *Inorg. Chem.* **1986**, *25*, 1420−1431.
(33) Kessissoglou, D. P.; Butler, W. M.; Pecoraro, V. L. *Inorg. Chem.* **1987**, *26*, 495−503.
(34) Coucouvanis, D.; Reynolds, R. A., III; Dunham, W. R. *J. Am. Chem. Soc.* **1995**, *117*, 7570−7571.

mT line, despite many efforts. The hyperfine pattern shown in Figure 8 exhibits up to 38 lines between 1.135 and 1.305 T that are regularly separated by 4.2−4.7 mT. Previously reported Q-band spectra recorded on model complexes[15,32] or on metalloproteins[7,13,36] exhibit similar hyperfine structures developed in the $g = 2$ region. The pattern observed here is detected at 8 K and is better resolved as the temperature increases. From this temperature dependence, it can be clearly attributed to the $S = 2$ spin state. The resolution is partially lost in the 1.230 T transition at 80 K. This may be attributed to the increasing contribution of the $S = 3$ state. No attempt was performed to simulate the frozen solution spectra, the overall profile being pretty close to the ones observed on powder samples.

Discussion

It has long been established that the EPR signature of dinuclear Mn(II) complexes is intricate due to the contribution of the different paramagnetic *S*-spin states with *S* ranging from 1 to 5. As mentioned in the Introduction, deconvolution methods have been applied to extract the relevant spin parameters. The methodology presented here relies on a scrupulous examination of the EPR spectra recorded at different temperatures. The starting hypothesis, common with the deconvolution approach, is that each spectrum can be reproduced by a linear combination of the individual spin state spectra, the weighted coefficients depending upon temperature according to eqs 6 and 7. We have shown in the results section that the spectra recorded between 6 and 30 K are indeed reproduced by a linear combination of two temperature-independent spectra, $Y_{S=1}(\nu,B)$ and $Y_{S=2}(\nu,B)$, calculated at X- and Q-bands with the same set of spin parameters, the contribution factors following the temperature dependence expected from the conjugated Boltzmann population of the S-ladder and the Curie behavior of each spin state (see eq 7). In addition, temperature effects within the $S = 1$ and $S = 2$ spin states were detected on the 4 or 5 K spectra that strongly affect the entire EPR profile. It is the first time to our knowledge that a series of dinuclear Mn(II) complexes EPR spectra are so well reproduced at both X- and Q-bands.

Deconvolution methods have been applied to the X-band EPR spectra of di-Mn(II) model complexes as well as catalases and arginase.[12,13] In these works, it is assumed that the main contributions to the EPR spectra originate from the $S = 1$ and $S = 2$ spin states. The temperature dependence of the weighted coefficients is thus constrained to the appropriate Boltzmann law for these spin states. Exchange coupling constants *J* were then determined but a recent investigation of the magnetization properties of the Mn-catalases from *Thermus thermophilus* and *Lactobacillus plantarum* revises downward these previously published values by a factor between 3 and 4.[37] Le Pape et al. attributed this discrepancy to an overestimation of the contribution of the $S = 1$ excited state to the overall EPR spectra. This remark could also apply to the di-Mn(II) model complex[12] investigated along this deconvolution process since no magnetization measurements have been run to check the EPR-derived *J*-value.

Indeed, the starting hypothesis relying on the $S = 1$ and $S = 2$ main contributions could be questioned if one looks to the extracted individual spin state spectra. A series of triplet spectra have been calculated by Mabbs and Collison assuming an isotropic Zeeman effect with $g = 2$ and different magnitudes of the zero-field splitting effect versus the excitation frequency within axial or rhombic symmetries.[29] No calculated profile approaches the proposed $S = 1$ spectra. Only one extracted $S = 2$ spectrum is tentatively analyzed assuming an axial zero-field splitting effect by comparison of the dependence of the resonant field values ($B \parallel z$ and $B \perp z$) upon the spin parameter $D_{S=2}$.[12] A calculation using the proposed spin parameters shows an important discrepancy with the proposed $S = 2$ spectrum, suggesting that if the proposed $S = 2$ spectrum is correct, a rhombicity in the zero-field splitting effect has to be introduced.

Considering the local zero-field splitting effects on the two Mn(II) ions in conjunction with the coupling interactions (isotropic and anisotropic components of exchange interaction and dipolar coupling) is the best way to correctly reproduce the variation of the spectra upon temperature. In particular, this will allow one to take correctly into account the changes in the relative line intensities within one spin state. This approach has been previously followed,[13,38] and to reduce the number of unknowns, the anisotropic exchange interaction was set to zero and the Mn(II) zero-field splitting tensors were considered of axial symmetry. Moreover, they were taken to be identical on both ions and collinear to the axial dipolar coupling tensor. Those constraints lead to poor simulations of the experimental spectra. Indeed, within this framework, the zero-field splitting $\tilde{D}_S$ tensors are of axial symmetry and share the same principal axis since they are related to the local $\tilde{D}_A$ and $\tilde{D}_B$ and to the coupling $\tilde{D}_{AB}$ tensors according to the following formula,[28]

$$\tilde{D}_S = d_A(S)\tilde{D}_A + d_B(S)\tilde{D}_B + d_{AB}(S)\tilde{D}_{AB} \qquad (13)$$

with

$$d_A(S) = d_B(S) = \frac{3S(S+1) - 3 - 4S_i(S_i+1)}{2(2S+3)(2S-1)} \qquad (14)$$

and

$$d_{AB}(S) = \frac{S(S+1) + 4S_i(S_i+1)}{2(2S+3)(2S-1)} \qquad (15)$$

where S_i is the local electronic spin with a $^5/_2$-value. From the equality of the $d_A(S)$ and $d_B(S)$ coefficients, eq 13 indicates that the resultant tensor $\tilde{D}_c = \tilde{D}_A + \tilde{D}_B$ is accessible. It has been elegantly demonstrated by Ozarowski et al.[39] in

(35) Antanaitis, B. C.; Brown, R. D., III; Chasteen, N. D.; Freedman, J. H.; Koenig, S. H.; Lilienthal, H. R.; Peisach, J.; Brewer, C. F. *Biochemistry* **1987**, *26*, 7932−7937.
(36) Poyner, R. R.; Reed, G. H. *Biochemistry* **1992**, *31*, 7166−7173.
(37) Le Pape, L.; Perret, E.; Michaud-Soret, I.; Latour, J.-M. *J. Biol. Inorg. Chem.* **2002**, *7*, 445−450.
(38) Schultz, B. E.; Ye, B.-H.; Li, X.-y.; Chan, S. I. *Inorg. Chem.* **1997**, *36*, 2617−2622.

a detailed investigation of isoelectronic dinuclear Fe(III) mono-μ-oxo complexes that the $\tilde{D}_c$ and $\tilde{D}_{AB}$ tensors are not collinear. Taking $\tilde{D}_c$ and $\tilde{D}_{AB}$ coaxial is thus a too restrictive framework. Moreover, the proposed coupling $\tilde{D}_{AB}$ tensors are rhombic, clearly indicating that they do not reduce to the dipolar coupling (isotropic *g*-tensors) and that the anisotropic component of the exchange interaction cannot be ignored.

We attempted to determine $\tilde{D}_c$ and $\tilde{D}_{AB}$ tensors from the knowledge of the sole eigenvalues of the $\tilde{D}_{S=1}$ and $\tilde{D}_{S=2}$ tensors, keeping in mind that these tensors are not necessarily collinear. The space parameter to be explored is still too large unless the constraint of the axiality of the coupling tensor $\tilde{D}_{AB}$ is added. We are currently working on this approach that will be validated by the determination of the $\tilde{D}_{S=3}$ tensor.

Hyperfine structure was detected at X-band on the 4.3 K spectrum recorded on a powder sample of **1**. From the temperature behavior, it is attributed to the $S = 2$ state and this assignment is indeed corroborated by the investigation of the acetonitrile frozen solution. The best resolved hyperfine pattern detected at 100 K on the frozen solution indeed coincides in position with the lines that are hyperfine-structured at 4.3 K (powder spectrum). At Q-band, no hyperfine interaction with the manganese nuclei was detected on the frozen solution sample within the $S = 1$ state but only within the $S = 2$ level. A nice analysis of the 1.0−1.4 T region has been recently reported by Howard et al. where the two equivalent manganese hyperfine couplings were taken into account for the $S = 2$ spectrum.[15] The dinuclear Mn(II) complex investigated in ref 15, [(tmeda)(AcO)Mn(μ-OH$_2$)(μ-OAc)$_2$Mn(OAc)(tmeda)], exhibits at 7 K an intense line at 535 mT ($g = 4.52$) that is very similar in field position and in profile to what we observe at 5 K for complex **1**. In conjunction with the hyperfine structure detected at 4 K, this line was attributed to a $S = {}^5/_2$ trinuclear Mn(II) species. This assignment is very puzzling since an isotropic transition around $g = 4.3$ arising from a $S = {}^5/_2$ system originates from the intermediate Kramers doublet, the $S = {}^5/_2$ state presenting a zero-field splitting effect characterized by a *E/D* ratio near 1/3 and a *D* parameter that exceeds in absolute value the microwave excitation energy. This last statement, if true at Q-band, still holds when going toward lower excitation frequency, that is, at X-band. But no transition in the $g = 4.3$ region with a symmetric line shape was detected at 9.42 GHz, invalidating the proposed attribution. In addition, lines separated by 2.6 mT were also detected on the transition located at 625 mT ($g = 3.87$) that cannot originate from the same $S = {}^5/_2$ species within the formulated hypothesis. A scrupulous examination of the recorded spectra (see also the Supporting Information of ref 15) suggest that the 535 mT transition is indeed associated with the $S = 1$ state of [(tmeda)(AcO)Mn(μ-OH$_2$)(μ-OAc)$_2$-Mn(OAc)(tmeda)] and the 625 mT line with the $S = 2$ state. Due to the smaller exchange interaction in this aquo-bridged complex, the $S = 1$ signature needs very low temperature to be detected without any contribution from the $S = 2$ spin state. It is thus more difficult to assign the detected transitions to the $S = 1$ and $S = 2$ spin states, respectively. It has to be noticed that the X-band spectra were recorded on a restrictive magnetic field range and that more transitions should be detected at higher field than 500 mT (see Figure 3 of ref 15). Investigation over a more extended field range would probably have allowed the detection of the most shifted $S = 1$ *z*-line and consequently the determination of the $D_{S=1}$ parameter.

Conclusion

We have presented here a detailed analysis of the EPR signature of a new X-ray structurally characterized di-Mn(II) complex presenting a μ-phenoxo-bis-μ-carboxylato core structure. An antiferromagnetic exchange interaction was evidenced by the variation of the molar magnetic susceptibility upon temperature and the fit of the experimental data led to a singlet−triplet separation of 9.6 cm^{-1}.

The present investigation has focused on two major points. The first one is the simulation of the EPR spectra recorded on a powder sample of [(Bpmp)Mn$_2$(μ-OAc)$_2$](ClO$_4$)·0.5H$_2$O at both X- and Q-bands between 6 and 30 K. In this temperature domain, only the two lowest $S = 1$ and $S = 2$ levels contribute significantly to the recorded signals. The original approach that has been exposed in this paper relies on a detailed examination of the variation upon temperature of the line intensities to identify the *S*-spin state from which these lines originate. Once the assignment is performed, the spin parameters are determined (in absolute value) and the temperature-independent *S*-spin state signatures are calculated using the XSophe program. Each experimental spectrum recorded at the temperature *T* may be accurately reproduced by a linear combination of these $S = 1$ and $S = 2$ traces and it is possible to deduce the exchange coupling constant from the temperature dependence of the determined weighted factors.

The second main point of the present study is the determination of the sign of the zero-field splitting parameters $D_{S=1}$ and $D_{S=2}$ from the line intensities of the 4 or 5 K spectrum.

The use of two microwave frequencies give strong confidence with respect to the proposed spin parameter values. A high-field high-frequency study is currently underway to confirm the negative sign of the $D_{S=2}$ parameter and to determine the $S = 3$ spin parameters in conjunction with the presented X- and Q-band investigations. This will allow the calculation of the local zero-field splitting tensor of the two Mn(II) ions and of the interaction tensor associated with the dipolar coupling and the antisymmetric exchange interaction.

We have recently obtained a series of dinuclear Mn(II) complexes using derivatives of the BpmpH ligand, the phenolic para methyl group being substituted by electron-withdrawing or electron-donating groups.[40] Preliminary results show that the exchange coupling constant varies

(39) Ozarowski, A.; McGarvey, B. R.; Drake, J. E. *Inorg. Chem.* **1995**, *34*, 5558−5566.

(40) Blanchard, S.; Blain, G.; Rivière, E.; Nierlich, M.; Blondin, G. Accepted in *Chem. Eur. J.*

among the series as the zero-field splitting effects within the triplet and the quintet spin states. The method for analyzing the EPR spectra that has been developed here will be applied to this series. This will give a unique opportunity to correlate the zero-field splitting parameters to structural features.

Acknowledgment. We are grateful to Dr. Alain Boussac (Service de Bioénergétique, URA CNRS 2096, CEA Saclay, Gif-sur-Yvette, France) for EPR facilities and helpful discussions. We thank the Conseil Régional de l'Ile de France for its contribution to the acquisition of the Bruker ELEXSYS X- and Q-band EPR spectrometer. The COST D21 European action and the LRC-CEA project are acknowledged for their financial support.

Supporting Information Available: Complete X-ray crystallographic data for **1**(ClO_4)·(C_2H_5)$_2$O in CIF format. $\chi_M = f(T)$ and $\chi_M T = f(T)$ plots where χ_M is the molar magnetic susceptibility of **1**(ClO_4)·0.5H_2O with theroretical curves (Figure S1), variation upon temperature of the Boltzmann population of any Zeeman level of one S-spin states ($1 \leq S \leq 5$) evaluated at zero field according to eq 7 with $J = 9.6$ cm^{-1} (Figure S2), and experimental and simulated spectra recorded at 28.2 K at X-band and at 12.5 and 25 K at Q-band (Figure S3). Variations of the energies of the Zeeman levels of a triplet state as a function of the applied magnetic field along the principal directions of the zero-field splitting tensor (Figure S4). This material is available free of charge via the Internet at http://pubs.acs.org.

IC0301066